Journal of Nuclear Materials 406 (2010) 113–118

Contents lists available at ScienceDirect

Journal of Nuclear Materials

journal homepage: www.elsevier.com/locate/jnucmat

Effect of prior crack growth on cleavage fracture of low toughness precracked Charpy specimens

M. Scibetta

SCK-CEN, Boeretang 200, B-2400 Mol, Belgium

A B S T R A C T

Cleavage fracture of reactor pressure vessel steels in the upper ductile to brittle transition region generally occurs with prior significant ductile crack growth. For low upper shelf materials and using PreCracked Charpy v-notch (PCCv) specimens that can be obtained from conventional surveillance programs, the effect of prior crack growth could be particularly important. In practice, the shape of the Master Curve and the failure distribution could be affected by ductile crack growth. To quantify the effect in practical applications, the effect of prior ductile on cleavage is evaluated on PCCv specimen.

The methodology use finite element calculations to grow a ductile crack and infer the brittle failure probability using the local approach to fracture. It is found that for very low upper shelf toughness materials, ductile crack growth enhances the failure probability, induces a steeper failure distribution and affects the shape of the Master Curve. However, for low toughness materials, the enhanced failure probability due to crack growth is compensated by loss of constraint.

1. Introduction

The vessel of a Pressurized Water Reactor (PWR) is an essential component for which integrity should be guaranteed throughout the lifetime of the reactor. In the core region, the Reactor Pressure Vessel (RPV) base material and welds are subject to high neutron fluence and thermal ageing, which can both induce embrittlement. In order to ensure safe operating conditions, the RPV-material properties are monitored within a mandatory surveillance program containing Charpy specimens made of representative RPV materials. The main purpose of this program is the evaluation of the fracture toughness within the ductile to brittle transition region and in the upper shelf. This approach is semi-empirical as fracture toughness is not measured directly but indexed from irradiation-induced changes in Charpy impact properties.

In recent years, new tools have become available and have been used to directly measure material fracture toughness from surveillance broken Charpy specimens [1]. The methodology is based on a combination of the reconstitution technology [2] and the Master Curve [3]. These techniques allow the fabrication of PreCracked Charpy v-notch (PCCv) specimens from broken halves and testing in the ductile to brittle transition regime, respectively.

For highly irradiated low upper shelf materials, ductile crack growth prior to brittle failure could invalidate the use of the Master Curve. It should be mentioned that for this reason the current ASTM E1921 [3] invalidates the results having more than 0.2 mm crack growth prior cleavage. It should be noted that in case of Charpy impact test in the middle of the ductile to brittle transition, ductile tearing always precede cleavage, therefore an approach such the one proposed in [4] should be used. In [5], a methodology has been developed and validated with experimental data in order to predict the effect of ductile crack growth on cleavage. For the ductile crack growth aspect, the methodology uses computational cells with Gurson–Tvergaard damage plasticity law [6]. Those cells contain a mechanism of progressive extinction when damage (i.e., void fraction) reaches a specified value. It should be noted that this methodology is sensitive to the mesh size [7,8] that is associated to mean spacing of the large void initiated by inclusions. This problem can be addressed using newly developed approaches [9], however, such approaches are still in the development stage and are not readily available in standard finite element codes. To predict the brittle failure probability in [5], the Beremin weakest link model [10] is used. The approach developed in [5] has been applied to deep and shallow crack Single Edge Bend (SE(B)) geometry and to Small Scale Yielding (SSY) configuration. The important points that were discussed in [5] are that both constraint loss and ductile tearing affect the failure probability. In particular, ductile tearing partially restores the near-tip constraint. This effect is significant for low constraint conditions and not very significant for high constraint conditions.

The 2D modeling developed in [5], was improved with 3D modeling in [11] and independently in [12]. The selected ductile damage model in [11] is based on computational cells but uses a

E-mail address: mscibett@sckcen.be

0022-3115/$ - see front matter © 2010 Elsevier B.V. All rights reserved.
doi:10.1016/j.jnucmat.2010.03.020

modified Lemaitre approach developed in [13]; in [12] the Rousselier model [7] is used. The failure probability of a one inch thickness compact tension specimen, 1T-C(T), as a function of the stress intensity factor shows a two-slope feature. The reduction of failure probability at higher stress intensity cannot be attributed to ductile crack growth but most probably to loss of constraint.

An even more advanced approach was developed in [14]; equidistant discrete voids are introduced in the model on the crack plane. Inter-porosity ligament ruptures according to a specified void volume fraction. This approach is even more computationally intensive and allows comparison with the previous developed computational cell approach from [5]. In particular results obtained in the SSY configuration reveal the effect of micro-mechanical parameters such as initial void fraction and void inter-distance.

To quantify the effect of prior ductile crack growth on cleavage in practical applications for the nuclear industry, the detailed study of the PCCv specimens is more important than the theoretical SSY configuration, the standard 1T-C(T) specimen or the generic SE(B) specimen. Therefore, this study will focus on this particular geometry. In former studies [4,5,11,12,14], the identification of micro-mechanical ductile failure parameters was required. This identification is time consuming and requires additional specific experiments and/or micro-structural investigations. Therefore, in this work a simplified approach is proposed.

2. Methodology

The methodology is based on finite element computations that allow crack propagation through node release. The goal of this paper is not to predict absolute material toughness. Such an approach would require the onerous and tedious identification of several micro-mechanical parameters from testing of non-fracture toughness specimens (e.g., tensile, notched tensile...) and eventual microstructure investigations.

Instead, the method presented here focuses on transferability and to the effect of prior ductile crack growth on brittle failure. Therefore, a more straightforward approach is used. It is supposed that the brittle and ductile failure behavior is known on the reference geometry selected as a one inch thick compact tension specimen 1T-C(T). Those results are transferred to the PCCv geometry by combining the two fracture mechanisms to predict the effect of ductile crack growth on brittle failure. The crack resistance curve is assumed as a material property and nodes are released accordingly to allow the crack to propagate. As ductile crack growth is much less sensitive to loss of constraint compared to brittle fracture, it is not necessary to identify micro-mechanical parameters for ductile fracture and the crack resistance curve can be considered as a material property valid for both 1T-C(T) and PCCv. This is also acknowledged in testing standards that allow the use of smaller specimens to measure a given level of ductile initiation J_{Ic} toughness [15] with respect to the size needed to measure an equivalent level of brittle initiation level K_{Jc} [3]. In case the methodology developed in [5] would be applied, it would result in identifying (i.e., fitting) micro-mechanical parameters in order to reproduce the crack resistance curve of the material. Those parameters are used subsequently to let the crack grow in the numerical simulations. In the domain of application envisaged in this paper, this does not provide additional benefit as the initial crack resistance curve should be produced after the numerical simulation.

The modeling of brittle failure used in this study is identical to the original Beremin model used in [5]. There exist many other models such as the Bordet model [16], the Prometey model [17], the Anderson and Dodds model [18] or the WST model [19]. All models are based on the weakest link principle and yield similar trends. However, the differences come from the level of complexity to identify the parameters needed. For engineering applications, it is felt that the Beremin model is sufficient. The Weibull stress is defined as [10]:

$$\sigma_W^m = \int_{V_p} \sigma_1^m \frac{dV}{V_0} \tag{1}$$

where V_0 is a reference volume taken equal to 50^3 μm^3, σ_1 the maximum principal stress, m the Weibull exponent that typically ranges from 5 to 20 and V_p the volume of integration for which the plastic deformation is larger than zero. In [20], a parametric study is performed to study the effect of loss of constraint. In particular Weibull exponents of 5, 10 and 20 are selected. It is found that the results, general trend and conclusions are not very sensitive to the selected Weibull exponent. On the other hand, the identification of the Weibull exponent on actual materials is not trivial as the problem is ill-conditioned when trying to identify m on high constraint configurations [21,22]. Therefore, in this study a typical value of 10 is selected for the Weibull exponent.

According to the model, the failure probability is a simple function given by:

$$F = 1 - \exp(-(\sigma_W/\sigma_u)^m) \tag{2}$$

where F is the failure probability and σ_u the cleavage stress. The cleavage stress can also be defined as the value of the Weibull stress at which the failure probability is 63.2% or at which the surviving probability is 36.8%.

3. Finite element model

In order to model actual material behavior, the incremental theory of plasticity is used in combination with an isotropic strain-hardening model. This is based on the Von Mises criterion, with a uniaxial true stress versus true strain function described by a power law:

$$\frac{\sigma}{\sigma_{YS}} = \begin{cases} \frac{\varepsilon}{\varepsilon_{YS}} & \text{if } \sigma < \sigma_{YS} \\ \left(\frac{\varepsilon}{\varepsilon_{YS}}\right)^n & \text{if } \sigma \geqslant \sigma_{YS} \end{cases} \tag{3}$$

$$\text{with } \varepsilon_{YS} = \sigma_{YS}/E \tag{4}$$

where E is the Young's modulus, σ_{YS} the yield strength, n the strain-hardening exponent, σ the true stress and ε the true strain.

The actual true stress versus true strain behavior of metallic materials can generally be fitted by a power law. Alternatively, the strain-hardening exponent can be obtained from the following Eq. (5), which can easily be solved with a non-linear iterative solver. This expression was derived in [23] by solving the instability point and converting true stress to engineering stress.

$$\frac{\sigma_{TS}}{\sigma_{YS}} = \frac{\left(\frac{n}{\varepsilon_{YS}}\right)^n}{\exp(n)} \tag{5}$$

where σ_{TS} is the ultimate tensile strength.

This study is limited to three materials, representing typical very low, low and high toughness ferritic steels. The designation for the two materials is VLT, LT and HT, respectively. Both materials have Young's modulus $E = 207$ GPa and Poisson's ratio $\nu = 0.3$. The VLT and LT materials have a hardening exponent $n = 0.05$, and Young to yield stress ratio $E/\sigma_{YS} = 350$. For the HT material $n = 0.1$ and $E/\sigma_{YS} = 500$. The crack resistance curve of the material is described by a power law function of the form:

$$J = C_1 \Delta a^{C_2} \tag{6}$$

where J is the J-integral in kJ/m^2, Δa is the crack extension in mm, C_1 and C_2 are material constants.

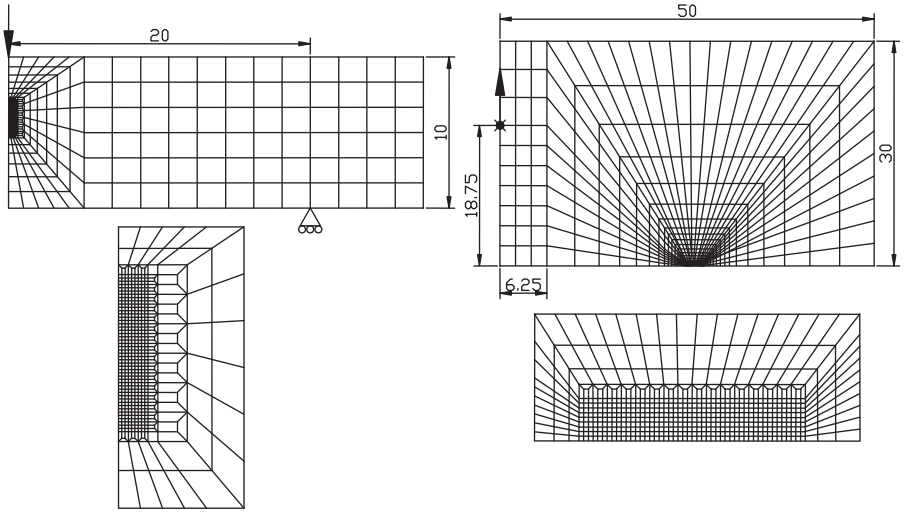

Fig. 1. Meshing of a PCCv (left) and 1T-C(T) (right) specimen and zoom at the crack tip location.

The VLT material has $C_1 = 100$ and $C_2 = 0.3$, the LT material has $C_1 = 400$ and $C_2 = 0.3$ while the HT material has $C_1 = 500$ and $C_2 = 0.5$.

Due to external constraints, a less representative 2D plane strain model is used instead of a computationally heavy 3D model. 8-Node isoparametric quadrilateral elements with reduced Gauss integration are used. Because large geometry changes and large strain are to be expected, the modified updated Lagrangian [24] procedure is used.

This study is limited to 1T-C(T) and PCCv specimens. In both cases a very common initial crack size to specimen width ratio of $a_0/W = 0.5$ is selected. Due to symmetry considerations, only half of the geometry needs to be considered, thus significantly reducing the required computational time.

Force is applied through contact between the specimen and the loading pins. Modeling these contact conditions in a finite element model is rather complex and introduces additional highly non-linear equations. As these conditions are not essential, the boundary conditions are simplified. The loading pin is simulated by imposing the displacement at the node in contact with the pin. In order to avoid large deformation of these elements, the hole for the pin is removed and the material properties are set to fully elastic for an area up to 6.25 mm from the load-line for the 1T-C(T). The notches machined for precracking and for clip gauge attachment are not included in the model, as these do not affect the results.

In order to model the geometry, a simple regular mesh could be used. However, this would increase the required computational time for a given accuracy. The preferred strategy is to use a fine meshing in deformed regions and a coarse mesh in regions that are less deformed. The mesh density is selected based on the experience gained from previous finite element calculations [25,26]. For information, the mesh of the 1T-C(T) (see Fig. 1) contains 1102 elements and 3429 nodes. For both geometries, the dimension of the smallest element located at the crack tip is 50 μm. This enables to divide a 2 mm crack extension in 40 steps using a node release technique.

After each step, the J-integral is calculated from force, load-line displacement and actual crack size as the sum of the elastic and plastic components. The plastic part is calculated incrementally using Eq. (7) given in ASTM E1820 [15]:

$$J_{\mathrm{pl}(i)} = \left[J_{\mathrm{pl}(i-1)} + \frac{\eta_{(i-1)}}{b_{(i-1)}}\frac{A_{\mathrm{pl}(i)} - A_{\mathrm{pl}(i-1)}}{B_{\mathrm{N}}}\right]\left[1 - \gamma_{(i-1)}\frac{a_{(i)} - a_{(i-1)}}{b_{(i-1)}}\right] \tag{7}$$

where b is the ligament size, a the crack size, B_{N} the net thickness, A_{pl} the plastic area (energy); η and γ are geometry dependent functions of the ligament to width ratio.

Crack extension is inferred from Eq. (6). When crack extension is larger than an element size, the nodes of this element are released to extend the crack.

The finite element code used, SYSWORLD, is a standard commercial code developed by the ESI group [24]. Due to the small size of the problem, the direct matrix inversion algorithm is selected. The solution of non-linear equations is performed using the BFGS[1] algorithm. The number of force increments is typically 250. The convergence for each increment is obtained in about 45 iterations. Triangulation is performed for every iteration to ensure convergence for elements that left the plastic domain due to node release.

The platform used for this project is a standard 3 GHz Pentium 4 PC running under Windows XP. The central process unit (CPU) time per force increment is 3.8 s. The total execution time is higher than the indicated CPU time because the management of the operating system and the pre- and post-processing time are not taken into account.

4. Finite element analysis

The finite element analysis provides force versus displacement results. These curves, given in Fig. 2, display a linear region followed by plasticity and a decreasing force due to crack propagation. These curves are typical of actual fracture toughness tests. The HT material displays a lower general yield but has the largest toughness which is in agreement with the selected material properties. The small oscillations observed for the PCCv geometry is due to rapid force drops due to crack jump extensions of 50 μm corresponding to one node release. Total elongation is the largest for the HT material which is to be expected from the specified material behavior law.

In Fig. 3, J-integral is calculated from the force versus displacement record and from the actual crack size using Eq. (7). This figure allows verifying that the calculations reproduce the specified material properties for the HT, LT and VLT. In addition and for comparison purposes, the J–R curve of an actual very low toughness material is given. The so-called JSPS material is an A553B Cl.1 steel

[1] Broyden, Fletcher, Goldfarb, and Shanno.

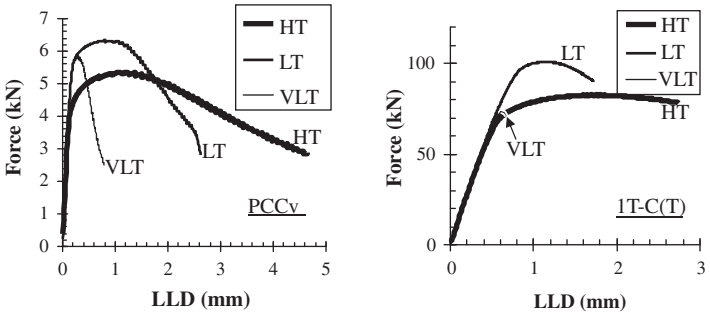

Fig. 2. Force versus Load-Line Displacement (LLD) records obtained from the computations.

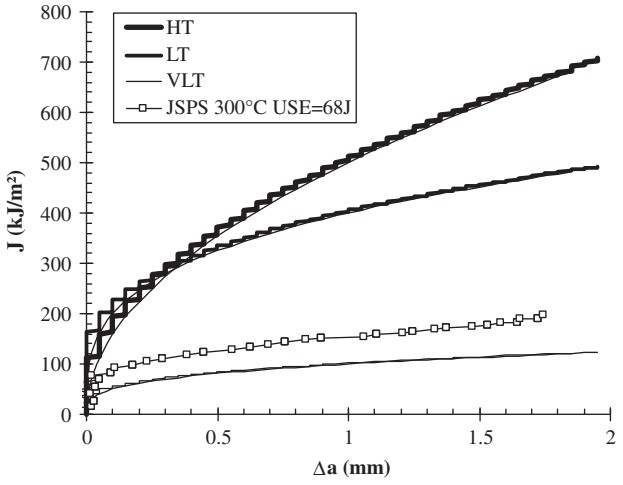

Fig. 3. Crack resistance curve calculated from the force versus displacement data from the C(T) finite element calculation compared to actual data on JSPS material.

which was used in a Round-Robin organized by the Japan Society for the Promotion of Science (JSPS) [27,28]. This steel is characterized by a remarkably low value of upper shelf energy in the unirradiated state.

As only very limited crack growth in the transition region is observed using the HT material, the rest of the study only concentrates on the LT and VLT materials.

Using the finite element results from the 1T-C(T), assuming a Weibull exponent $m = 10$, and assuming that the shape of the Master Curve as a function of temperature is the one used in the ASTM standard E1921 [3], it is easy to identify the Weibull stress as a function of temperature (see Fig. 4). The value of the cleavage stress is identical for both the LT and VLT materials. The reason is that although the two materials have different resistance curves, the flow properties are identical. It should be noted that in this analysis the E/σ_{YS} ratio is taken as a constant independent of the test temperature. For actual material σ_{YS} will decrease with increasing temperature. Therefore, for actual material, the Weibull stress parameter will be less temperature dependent than shown in Fig. 4. In [25], even when the yield strength temperature dependence was taken into account, all participants found an increasing Weibull stress with temperature.

The identified cleavage stress at a particular temperature can be used to predict the failure probability of PCCv specimens using Eq. (2). An example is given in Fig. 5 for the LT material −40 and −75 °C below the reference temperature. The failure probability displays a three-slope trend. Between 70 and 190 MPa$\sqrt{}$m, the rate of failure probability decreases due to loss of constraint. The start of loss of constraint is identified at an M value of 100 which is consistent with previous 2D finite element studies [28]. M is a dimensionless parameter defined as $M = b\sigma_{YS}/J$. At 190 MPa$\sqrt{}$m, the failure probability increases due to the crack growth that compensates loss of constraint. The effect of crack growth increases the sampled plastic volume eligible to find a crack initiator and resharpen the crack tip. At the reference temperature the fracture toughness is strongly affected by loss of constraint. This is partly due to the fact that 2D finite element analysis shows stronger loss of constraint than 3D finite element calculations [29,30].

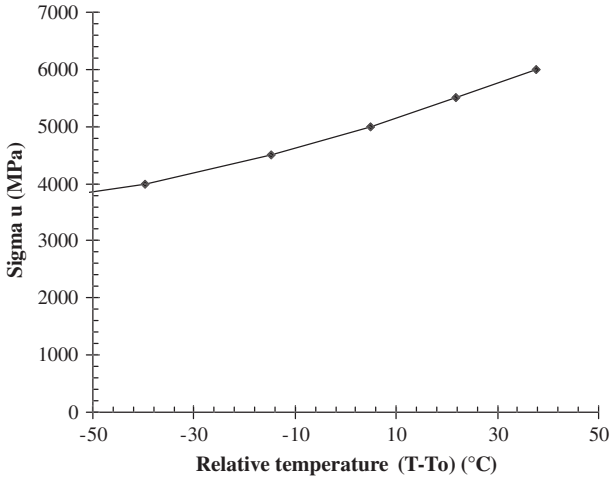

Fig. 4. Identification of the cleavage stress on the LT and VLT materials.

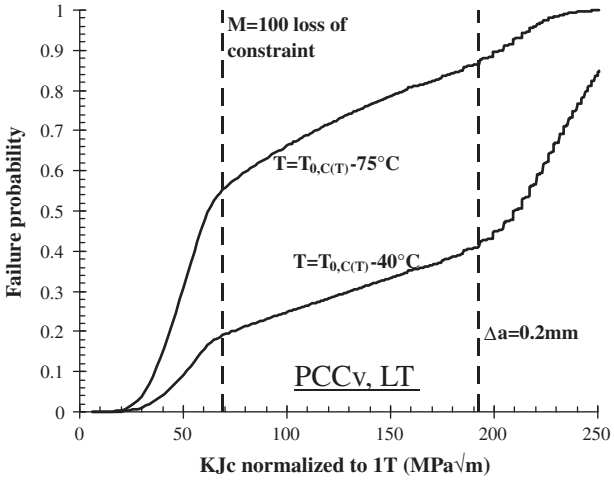

Fig. 5. Failure probability for the PCCv specimen of the LT material.

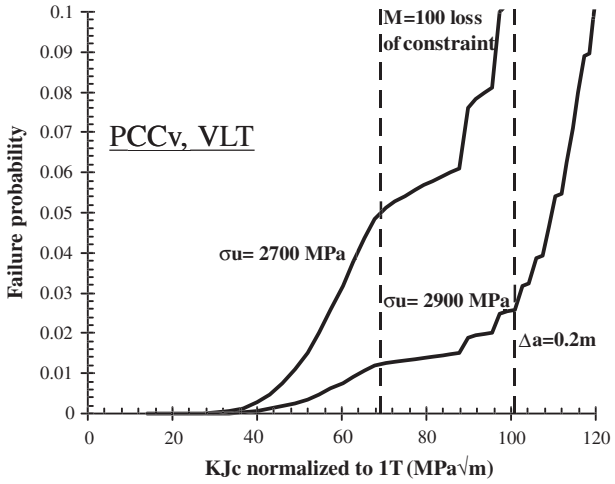

Fig. 6. Failure probability for the PCCv specimen VLT material.

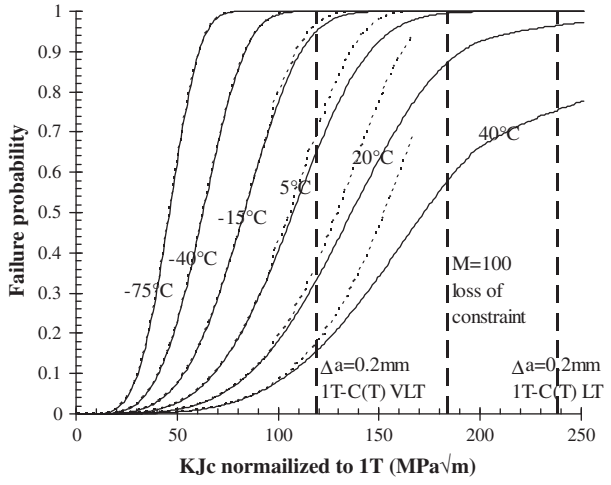

Fig. 7. Failure probability for the 1T-C(T) specimens of the LT and VLT materials. Dotted lines correspond to the failure probability of the VLT material and continuous lines correspond to the failure probability of the LT material.

For the VLT material, the failure probability is given in Fig. 6. The three-slope trend is also observed. Each crack growth extension of 50 μm directly increases the failure probability and introduces artificial steps in the failure probability.

The failure probability for 1T-C(T) specimens for the LT and VLT materials is compared in Fig. 7. In this case the failure probability is strongly affected by the loss of constraint as most of the results are below the $M = 100$ limit. However, the failure probability for the 1T-C(T) specimen is affected by the presence of crack growth that is present for the VLT material (dotted lines).

Using the failure probability given in Fig. 7, the percentile of 5%, 50% and 95% can be selected to derive the Master Curve shape of the 1T-C(T) specimen for the LT and VLT materials. Fig. 8 shows that for the LT material the 95% percentile is above the Master Curve, which can be attributed to loss of constraint. Instead for the VLT material the 95% percentile is below the Master Curve, which can be attributed to ductile crack growth. The 5% percentile curve, which is generally of interest for safety assessment purposes, is not affected by loss of constraint or ductile crack growth. In order to evaluate the quality of the qualitative model, 70 PCCv from the JSPS material [28] are compared in Fig. 8. It should be noted that data points above 150 $MPa\sqrt{m}$ shows ductile crack

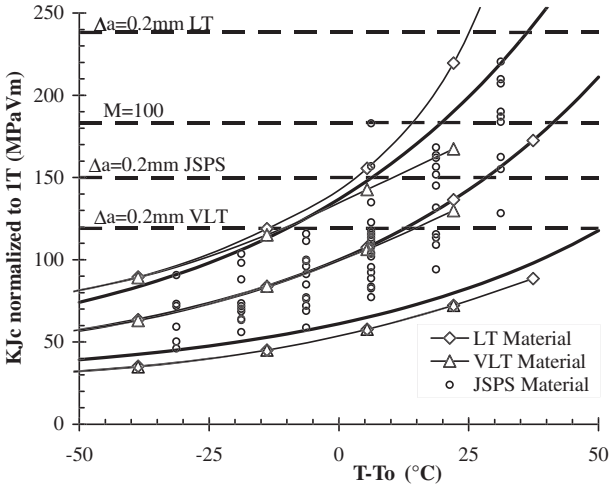

Fig. 8. Master Curve shape for 1T-C(T) specimens of the LT and VLT materials. Solid curves correspond to the Master Curve per ASTM E1921 [3].

growth prior cleavage fracture. The JSPS material has a toughness between the LT and the VLT model materials. Therefore, according to the model the loss of constraint should be compensated by ductile crack growth. This is indeed what can be observed Fig. 8 as the original Master Curve describes the JSPS data very well in the whole transition region.

5. Conclusions

A simplified methodology to model brittle failure in the presence of ductile crack growth has been successfully applied to PCCv and 1T-C(T) specimens. The main findings are summarized as follow.

- For PCCv specimens, the failure probability displays a three-slope trend. The first slope change is due to loss of constraint that reduces the failure probability. The second slope change is due to crack growth that increases failure probability.
- Crack growth is very effective in increasing the failure probability due to crack sharpening and to the increased volume eligible to provide a cleavage initiator. However, its effect is limited (even for very low toughness materials) due to the level of fracture toughness at which this phenomenon appears. Consequently, the lower bound fracture toughness (5% percentile) is practically unaffected by crack growth.
- For the 1T-C(T) specimen and for very low toughness materials, the effect of ductile crack growth on cleavage can occur prior to loss of constraint. In practice, only the 95% percentile failure is affected. The curve slope increase due to loss of constraint and decreases due to crack growth.
- The model is found in accordance with experimental PCCv fracture toughness data obtained on the JSPS low upper shelf material.

References

[1] E. Lucon, M. Scibetta, R. Chaouadi, E. van Walle, R. Gérard, Int. J. Press. Vessels Pip. 84 (9) (2007) 536–544.
[2] ASTM Standard E1253, Standard Guide for Reconstitution of Irradiated Charpy-sized Specimens, ASTM International, West Conshohocken, PA, 2007, Available from: <www.astm.org>.
[3] ASTM Standard E1921, Standard Test Method for Determination of Reference Temperature, To, for Ferritic Steels in the Transition Range, ASTM International, West Conshohocken, PA, 2008, Available from: <www.astm.org>.
[4] B. Tanguy, J. Besson, R. Piques, Eng. Fract. Mech. 72 (3) (2005) 413–434.

[5] C. Ruggieri, R.H. Dodds Jr., Int. J. Fract. 79 (4) (1996) 309–340.
[6] V. Tvergaard, A. Needleman, Acta Metall. 32 (1984) 157–169.
[7] G. Rousselier, Nucl. Eng. Des. 105 (1987) 97–111.
[8] A. Gullerud, X. Gao, R.H. Dodds Jr., R. Haj-Ali, Eng. Fract. Mech. 66 (1) (2000) 65–92.
[9] J. Mediavilla, R.H.J. Peerlings, M.G.D. Geers, Eng. Fract. Mech. 73 (7) (2006) 895–916.
[10] F.M. Beremin, Metall. Trans. A 14A (1983) 2277–2287.
[11] L. Esposito, D. Gentile, N. Bonora, Eng. Fract. Mech. 74 (4) (2007) 549–562.
[12] S. Carassou, Cleavage Onset in a Low Alloy Steel: Influence of Ductile Damaged Zones around Inclusions, PhD Thesis, Ecole nationale supérieure des mines de Paris, France, 1999, pp. 1–255 (in French).
[13] N. Bonora, Eng. Fract. Mech. 58 (1–2) (1997) 11–28.
[14] J.P. Petti, R.H. Dodds Jr., Int. J. Solids Struct. 42 (13) (2005) 3655–3676.
[15] ASTM Standard E1820, Standard Test Method for Measurement of Fracture Toughness, ASTM International, West Conshohocken, PA, 2008, Available from: <www.astm.org>.
[16] S.R. Bordet, A.D. Karstensen, D.M. Knowles, C.S. Wiesner, Eng. Fract. Mech. 72 (3) (2005) 435–452.
[17] B.Z. Margolin, V.A. Shvetsova, A.G. Gulenko, V.I. Kostylev, Eng. Fract. Mech. 75 (11) (2008) 3483–3498.
[18] T.L. Anderson, R.H. Dodds Jr., Simple constraint corrections for subsize fracture toughness specimens, in: W.R. Corwin, F.M. Haggag, W.L. Server (Eds.), Small Specimen Test Techniques Applied to Nuclear Reactor Vessel Thermal Annealing and Plant Life Extension, ASTM International, West Conshohocken, PA, ASTM STP 1204, 1983, pp. 93–105.
[19] K. Wallin, A. Laukkanen, Eng. Fract. Mech. 75 (11) (2008) 3367–3377.
[20] M. Scibetta, J. Schuurmans, E. Lucon, J. ASTM Int. 5 (9) (2008) 1–14.
[21] J.P. Petti, R.H. Dodds Jr., Eng. Fract. Mech. 72 (1) (2005) 91–120.
[22] C. Ruggieri, X. Gao, R.H. Dodds Jr., Eng. Fract. Mech. 67 (2000) 101–117.
[23] M. Scibetta, Contribution to the Evaluation of the Circumferentially-Cracked Round Bar for Fracture Toughness Determination of Reactor Pressure Vessel Steels, Dissertation for the Degree of Doctor in Applied Sciences, Université de Liège, Belgium, March 1999.
[24] ESI Group, SYSTUS+ 2.0, Analysis Reference Manual, 1998.
[25] C. Poussard, ESIS TC8 – Numerical Round Robin on Micro Mechanical Models: Results of Phase III for the Simulation of the Brittle to Ductile transition Curve, Report CEA, DMN/SEMI/LCMI/NT/2003-035/A, 2004, pp. 1–78.
[26] M. Scibetta, E. Lucon, J. Schuurmans, E. van Walle, Eng. Fract. Mech. 73 (4) (2006) 524–534.
[27] Standard Test Method for Fracture Toughness within Ductile-Brittle Transition Range, Standard of the 129th Committee, Japan Society for the Promotion of Science, 1995 (in Japanese).
[28] E. Lucon, M. Scibetta, Assessment of the Master Curve Approach on Three Reactor Pressure Vessel Steels (JRQ, JSPS, 22NiMoCr37), Open Report SCK•CEN-BLG-869, SCK•CEN, Mol, Belgium, 2001
[29] T.L. Anderson, R.H. Dodds Jr., J. Test. Eval. 2 (1991) 123–134.
[30] M. Nevalainen, R.H. Dodds Jr., Numerical Investigation of 3-D Constraint Effects on Brittle Fracture in SE(B) and C(T) Specimens, Report UILU-ENG-95-2001, Department of Civil Engineering, University of Illinois at Urbana – Champaign Urbana, Illinois, February 1995